

Low-frequency spin qubit detuning noise in highly purified $^{28}\text{Si}/\text{SiGe}$

Tom Struck,¹ Arne Hollmann,¹ Floyd Schauer,² Olexiy Fedorets,¹ Andreas Schmidbauer,² Kentarou Sawano,³ Helge Riemann,⁴ Nikolay V. Abrosimov,⁴ Łukasz Cywiński,⁵ Dominique Bougeard,² and Lars R. Schreiber¹

¹*JARA-FIT Institute for Quantum Information, Forschungszentrum Jülich GmbH and RWTH Aachen University, Aachen, Germany*

²*Institut für Experimentelle und Angewandte Physik, Universität Regensburg, Regensburg, Germany*

³*Advanced Research Laboratories, Tokyo City University, Tokyo, Japan*

⁴*Leibniz-Institut für Kristallzüchtung (IKZ), Berlin, Germany*

⁵*Institute of Physics, Polish Academy of Sciences, Warsaw, Poland*

The manipulation fidelity of a single electron qubit gate-confined in a $^{28}\text{Si}/\text{SiGe}$ quantum dot has recently been drastically improved by nuclear isotope purification. Here, we identify the dominant source for low-frequency qubit detuning noise in a device with an embedded nanomagnet, a remaining ^{29}Si concentration of only 60 ppm in the strained ^{28}Si quantum well layer and a spin echo decay time $T_2^{\text{echo}} = 128 \mu\text{s}$. The power spectral density (PSD) of the charge noise explains both the observed transition of a $1/f^2$ - to a $1/f$ -dependence of the detuning noise PSD as well as the observation of a decreasing time-ensemble spin dephasing time from $T_2^* \approx 20 \mu\text{s}$ with increasing measurement time over several hours. Despite their strong hyperfine contact interaction, the few ^{73}Ge nuclei overlapping with the quantum dot in the barrier do not limit T_2^* , as their dynamics is frozen on a few hours measurement scale. We conclude that charge noise and the design of the gradient magnetic field is the key to further improve the qubit fidelity.

Gate-defined quantum dots (QDs) are a promising platform to confine and control single spins, which can be exploited as quantum bits (qubits)¹. Unlike charge, a single spin does not couple directly to electric noise. Dephasing is dominated by magnetic noise, typically from the nuclear spin bath overlapping with the QD². The use of silicon as a qubit host material boosted the control of individual spins by minimizing this magnetic noise: in addition to the intrinsically low hyperfine interaction in natural silicon, the existence of nuclear spin-free silicon isotopes, e.g. ^{28}Si , allows isotopical enrichment in crystals^{3,4}. Controlling individual electrons and spins in highly enriched ^{28}Si quantum structures^{5–8} then opens the door to an attractive spin qubit platform realized in a crystalline nuclear spin vacuum. Indeed, two-qubit gates^{9–11} have recently been demonstrated in natural and enriched quantum films, while isotopical purification of ^{28}Si down to 800 ppm of residual nuclear spin-carrying ^{29}Si allowed to push manipulation fidelities beyond 99.9% for a single qubit^{12,13} and towards 98% for two qubits¹⁴. Qubit manipulation of individual spins is currently either realized with local AC magnetic fields generated by a stripline to drive Rabi transitions^{6,7,15} or via artificial spin-orbit coupling engineered by a micromagnet integrated into the device. This latter approach is advantageous by allowing the control of spin qubits solely by local AC electric fields^{10–12,16}, permitting excellent local control and faster Rabi frequencies. At the same time it opens a new dephasing channel for electric noise, due to the static longitudinal gradient magnetic field of the micromagnet, competing with the magnetic noise. To fully exploit the potential of magnetic noise minimization through isotope enrichment in $^{28}\text{Si}/\text{SiGe}$, two experimental questions thus become relevant for devices with integrated static magnetic field gradients: Firstly, to what extent electronic noise impacts the spin qubit dephasing compared to magnetic noise¹⁷ and, secondly, which role the natural SiGe potential wall barriers play for dephasing, since the hyperfine interaction of bulk Ge exceeds the one of bulk Si by a factor of approximatively $100^{18,19}$.

Here, we present an electron spin qubit implemented in a highly isotopically purified $^{28}\text{Si}/\text{SiGe}$ device, with only 60 ppm of residual ^{29}Si , which includes a magnetic field gradient generated by a nanomagnet integrated into the electron-confining device plane. We use Ramsey fringe experiments to investigate the detuning noise spectrum of the single electron spin down to 10^{-5} Hz. We find the frequency dependence of the qubit detuning spectrum to be identical to the spectrum of the device's electric charge noise over more than 8 decades. At low frequencies, below $5 \cdot 10^{-3}$ Hz, both noise spectra decrease with $1/f^2$. Above, they transit to a $1/f$ dependence and finally present a behavior comparable to a device¹² featuring a micromagnet and 800 ppm ^{29}Si at higher frequencies, as deduced from a Hahn-echo sequence for the detuning, yielding $T_2^{\text{echo}} = 128 \mu\text{s}$. Electric noise thus dominates our qubit dephasing in a broad frequency range. It is also responsible for the observed decrease of T_2^* with increasing measurement time²⁰. Interestingly, although we show the ^{73}Ge in the quantum well-defining natural SiGe to represent a potential limitation for our device, our experiments suggest the nuclear spin bath to be frozen on a time scale of hours and to much less contribute to T_2^* than expected at the ergodic limit.

The device used for all measurements consists of an undoped $^{28}\text{Si}/\text{SiGe}$ heterostructure confining a two dimensional electron gas in ^{28}Si with 60 ppm of residual ^{29}Si . Metal gates are used to form a quantum dot (QD) containing a single electron (Fig. 1(a)). The charge state of the QD is detected via a single electron transistor (SET) located at the right-hand side of the device. The large gate labeled M on the left-hand side is a single domain Co nanomagnet. Its stray-magnetic field provides a magnetic field gradient²¹ for spin driving by electric dipole spin resonance (EDSR). For details of the device see the supplements and Ref.²². We apply an external magnetic field of 668 mT along the x -direction.

First, we focus on the PSD of the frequency detuning Δf of the qubit with respect to a reference frequency of $f_R = 19.9\text{GHz}$. Δf is determined by a Ramsey fringe measure-

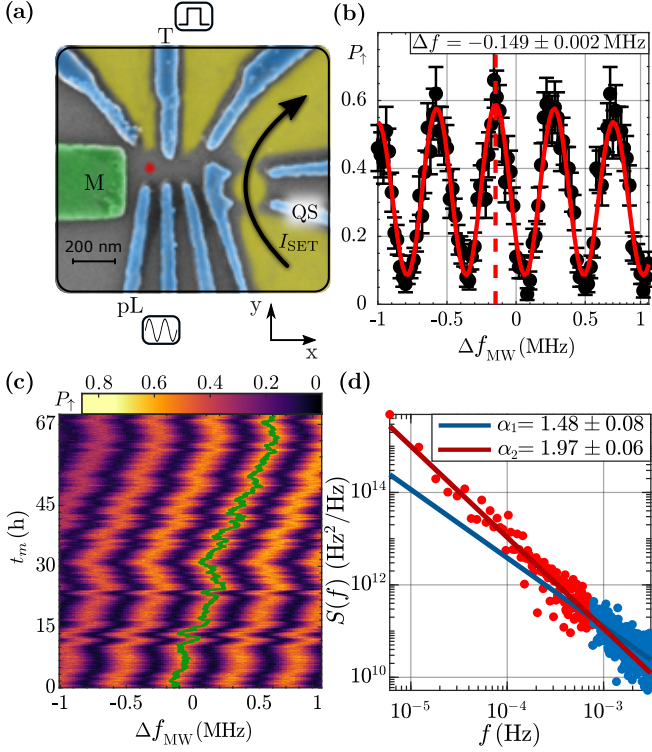


FIG. 1: (a) Colored scanning electron micrograph of a sample similar to the one used in this work. (b) Measurement of Ramsey fringes. The spin-up probability is recorded as a function of the resonance detuning Δf_{MW} . Each point corresponds to 100 single-shot measurements. The position of the spin resonance is indicated by the dashed red line. (c) Time evolution of the Ramsey fringe pattern during a measurement time $t_m = 67$ hours. The green solid line tracks the resonance detuning Δf extracted from the fringes. (d) PSD $S(f)$ of the qubit detuning calculated from the data shown in panel (c).

ment, during which the microwave pulses are detuned from the reference by Δf_{MW} (Fig. 1(b)). We vary Δf_{MW} from -1 to 1 MHz in 100 steps. Each point of the spin-up probability P_\uparrow is an average over 100 single-shot measurements. One Ramsey fringe, which is one measurement of Δf , takes 120 s. We fit Δf by applying the formula for the fringe pattern²³:

$$P_\uparrow(f_R, t_e, \Delta f, t_{\pi/2}) = \frac{4f_R^2}{\Phi^2} \cdot \sin\left(\pi t_{\pi/2} \Phi\right)^2 \cdot \left[\cos(\pi \Delta f t_e) \cdot \cos\left(\pi t_{\pi/2} \Phi\right) - \frac{\Delta f}{\Phi} \cdot \sin(\pi \Delta f t_e) \cdot \sin\left(\pi t_{\pi/2} \Phi\right) \right]^2 \quad (1)$$

where $\Phi = \sqrt{\Delta f^2 + f_R^2}$, t_e is the evolution time between the two $\pi/2$ gates and $t_{\pi/2}$ is the execution time of the $\pi/2$ gate.

Fig. 1(c) displays Ramsey fringes recorded during a measurement time period t_m of 67 hours. The green line tracks Δf during the full time period. We calculated the PSD $S(f)$ of the qubit detuning with Welch's method (Fig. 1(d)). For

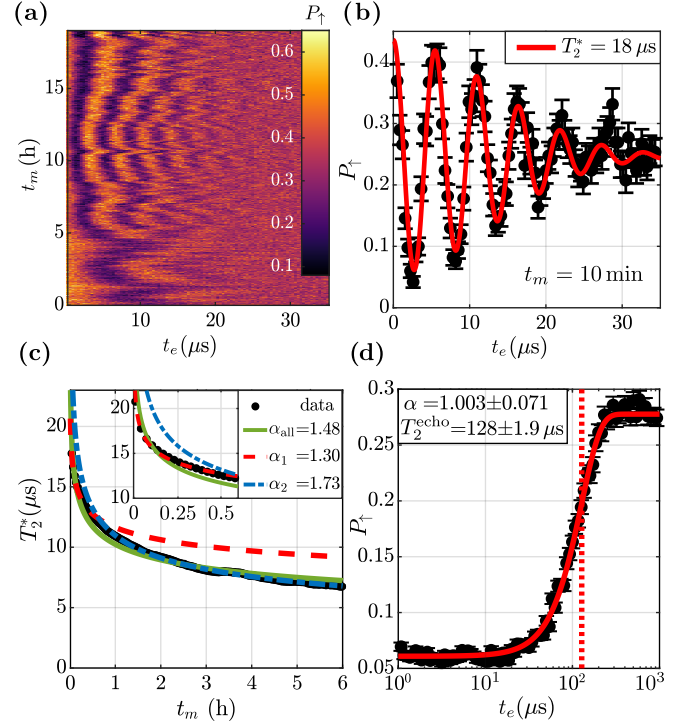


FIG. 2: (a) Time evolution of the T_2^* measurement. Each point is an average over 50 single-shot measurements. (b) Measurement of the spin-up probability as a function of the evolution time t_e . Each point corresponds to 500 single-shot measurements. The solid line shows a fit of a Gaussian decay revealing the time-ensemble dephasing time T_2^* . (c) Dependence of T_2^* on the measurement time. The solid green line shows a fit to all data points with one α -value. The red and blue lines show fits to the long and shorter measurement times. (d) Spin-up probability as a function of the evolution time t_e after a Hahn-echo gate sequence. Each point is an average over 5000 single shot measurements. The solid line is a fit to Eq. 4. The dashed line marks the fitted T_2^{echo} .

frequencies below $\approx 7 \cdot 10^{-4}$ Hz, we find a $S(f) \propto 1/f^{1.97}$ dependence. It transitions into a region with smaller exponent, here fitted with $S(f) \propto 1/f^{1.48}$ (blue line in Fig. 1(d)). Note that spin qubits in GaAs which dephase dominantly due to hyperfine interaction^{24–26} are also characterized by a $1/f^2$ dependence in their low-frequency detuning noise PSD, which has been assigned to nuclear spin diffusion there.^{27,28}

Having analyzed the qubit detuning noise $S(f)$ in the low-frequency regime, we now investigate its impact on the time-ensemble spin dephasing time T_2^* . We recorded P_\uparrow during a series of Ramsey sequences with varying t_e (Fig. 2(a)) in every line. For each t_m , we average as many consecutive $P_\uparrow(t_e)$ lines of this dataset as required to reach a total measurement time t_m . The averaged $P_\uparrow(t_e)$ was then fitted with

$$P_\uparrow(t_e) = A \cdot \exp\left(-\left(\frac{t_e}{T_2^*}\right)^2\right) \cos(2\pi \Delta f \cdot t_e) + B, \quad (2)$$

where A and B are constants related to the qubit initializa-

tion and readout fidelity. An example of $P_{\uparrow}(t_e)$ measured over $t_m = 10$ min is shown in Fig. 2(b). We extract $T_2^*(t_m = 10 \text{ min}) = 18 \mu\text{s}$. To achieve better statistics, this procedure was executed consecutively for different bundles of $P_{\uparrow}(t_e)$ lines. We chose to offset the bundles by 25 lines giving overlap between them. This results in each $T_2^*(t_m)$ value being averaged from 900 $T_2^*(t_m)$ values using different line bundles from the dataset displayed in Fig. 2(a) and a second dataset not shown here. Fig. 2(c) shows these averaged $T_2^*(t_m)$ for t_m ranging between 38 seconds and 6.3 hours. Remarkably, $T_2^*(t_m)$ drops monotonously with increasing measurement time without saturating for long t_m , qualitatively matching the qubit detuning noise PSD $S(f)$, which keeps increasing towards low frequencies (Fig. 1(d)). In a rough approximation, considering detuning noise of the type $S(f) = S_0/f^\alpha$ with $\alpha \gtrsim 1$, $T_2^*(t_m)$ induced by detuning noise is (see Supplement Notes 1):

$$T_2^*(t_m) = \left(\frac{4\pi^2 S_0}{\alpha - 1} (t_m^{\alpha-1} - t_e^{\alpha-1}) \right)^{-\frac{1}{2}}. \quad (3)$$

Fitting $T_2^*(t_m)$ with only one $\alpha_{\text{all}} = 1.48$ (green solid line) shows clear deviation from the data points (Fig. 2(c)). Motivated by the variation of α in $S(f)$, we fit two separate ranges of t_m above and below $t_m = 25$ min (that is $6.7 \cdot 10^{-4}$ Hz, which is very close to the transition point $7 \cdot 10^{-4}$ Hz found in Fig. 1(d)), which are characterized by $\alpha_1 = 1.30$ (red dashed curve) and $\alpha_2 = 1.73$ (blue dashed curve), and are in good qualitative agreement with α_1 and α_2 found for the detuning noise in Fig. 1(d). The quantitative deviation of both α_i ($i = 1, 2$) determined by the $T_2^*(t_m)$ compared to the ones directly fit to the PSD results from the fact that the T_2^* measurement integrates over the PSD from t_m^{-1} to t_e^{-1} .

Our spin-detection bandwidth in the Ramsey fringe experiment sets a limit on the maximum frequency of $S(f)$ in Fig. 1(d). To gain information on $S(f)$ at a higher frequency, we performed a Hahn-echo experiment, that is extended the Ramsey control sequence by a π_X gate between the two $(\pi/2)_X$ gates, in order to filter out low frequency noise. The measured data (Fig. 2(d)) has been fitted with

$$P_{\uparrow}(t_e) = A \cdot \left(1 - \exp \left(- \left(\frac{t_e}{T_2^{\text{echo}}} \right)^{\alpha+1} \right) \right) + B. \quad (4)$$

We find $\alpha = 1.003 \pm 0.071$ and $T_2^{\text{echo}} = 128 \pm 1.9 \mu\text{s}$. We can deduce that $S(f) \propto 1/f$ at a frequency of approximately $f = 1/T_2^{\text{echo}} = 7.8 \text{ kHz}$, in line with the observations in a device with an on-chip micromagnet and 800 ppm residual ^{29}Si for $f > 10^{-2} \text{ Hz}$ ¹². With the low-frequency PSD (Fig. 1(d)) and these spin echo results we conclude that the initial $S(f) \propto 1/f^2$ dependence observed at low frequencies transits to a $S(f) \propto 1/f$ dependence around $7 \cdot 10^{-4} \text{ Hz}$ to $1 \cdot 10^{-3} \text{ Hz}$. With the detection bandwidth limit set by the Ramsey fringe experiment at approximately $3 \cdot 10^{-3} \text{ Hz}$, we observe this gradual transition, explaining $\alpha = 1.48$ found in Fig. 1(d). Remarkably, we find a 28 % higher T_2^{echo} compared to the

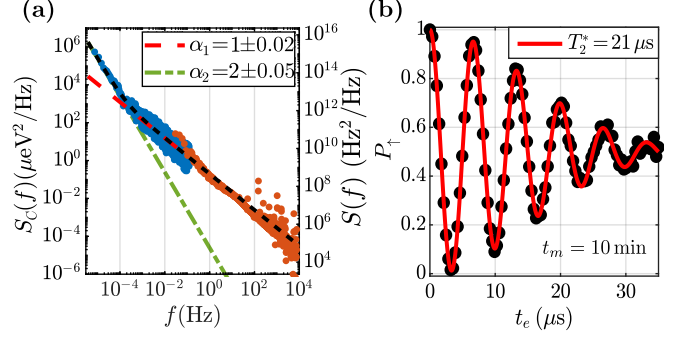


FIG. 3: (a) PSD of the charge noise determined by the noise of the current I_{SET} through the SET. The blue and the red dots represent two datasets. We read $S_C^{1/2}(1 \text{ Hz}) = 0.47 \mu\text{eV}/\sqrt{\text{Hz}}$ at 1 Hz. The right y-axis is converted into the PSD scale of detuning noise by Eq. 5. (b) Simulation of the spin-up probability as a function of the evolution time t_e taking the measured charge noise spectrum into account (black dots). T_2^* is fitted (red line) by the same fit function as in Fig. 2(b).

device with an on-chip micromagnet and 800 ppm residual ^{29}Si ¹², indicating that overall the detuning noise is lower in our sample in this regime.

In order to investigate the impact of charge noise, we measured the charge noise in the qubit vicinity via the current noise of the SET sensor. This current noise is translated into gate equivalent voltage-noise by the variation $dI_{\text{SET}}/dV_{\text{QS}}$ of the SET current by the voltage applied to the SET gate QS (see Fig. 1(a)). We measured the current noise ϵ_{SET} at a highly sensitive operation point of the SET and subtracted from its PSD the noise spectrum measured when the SET was set to be insensitive to charge noise from the device, in order to remove noise originating from the measurement circuit²⁹. Fig. 3(a) shows the measured PSD of the SET noise. As the data reveals two slopes, we fitted with $S_C(f) = S_{C1}/f^{\alpha_1} + S_{C2}/f^{\alpha_2}$. The fitted exponents of the $S_C(f)$ spectrum are $\alpha_1 = 1 \pm 0.02$ and $\alpha_2 = 2 \pm 0.05$, respectively, the transition being at about 10^{-3} Hz . This frequency dependence is in very good agreement with the one observed for the qubit detuning PSD in Fig. 1(d) and with the qualitative trend extended to high frequencies with the Hahn-echo experiment. Making the comparison more quantitative, we assume the charge noise at the SET to be similar to the one of the QD and the longitudinal gradient magnetic field to be isotropic for lateral QD displacements. Using the current noise trace $\epsilon_{\text{SET}}(t)$, the resulting frequency detuning is

$$\Delta f(t) = \epsilon_{\text{SET}}(t) \cdot \frac{dV_{\text{QS}}}{dI_{\text{SET}}} \cdot \frac{dx_{\text{QD}}}{dV_{\text{QD}}} \cdot \frac{dB_x}{dx_{\text{QD}}} \cdot \frac{g\mu_B}{\hbar}, \quad (5)$$

where $\frac{dV_{\text{QS}}}{dI_{\text{SET}}} = 1/35 \text{ mV/pA}$ is the inverse of the current change through the SET induced by a change of the voltage on the gate. $dx_{\text{QD}}/dV_{\text{QD}} = 0.024 \text{ nm/mV}$ is the estimated displacement of the QD induced by voltage changes on the adjacent gates according to an electrostatic device simulation.

$dB_x/dx_{QD} = 0.08$ mT/nm is the simulated isotropic longitudinal gradient magnetic field at the QD position. The factor $\frac{g\mu_B}{\hbar}$, containing the electron g-factor ($g \approx 2$), the Bohr magneton μ_B and the reduced Planck constant \hbar , converts magnetic field to frequency. We convert the charge noise PSD into qubit detuning noise by Eq. 5 (right y-axis in Fig. 3(a)). The low-frequency part of the PSD (blue dots in Fig. 3(a)), shows excellent agreement with the qubit detuning noise PSD $S(f)$ in its frequency dependence and its magnitude. In order to also include the high frequency range (red dots in Fig. 3(a)) into the comparison, we simulated the spin-up probability after a Ramsey gate sequence at time t_m with evolution time t_e using

$$P_{\uparrow}(t, t_e) = \frac{1}{2}(\cos(2\pi t_e \Delta f(t)) + 1) \quad (6)$$

and include quasi-static noise during the free evolution time t_e from the full PSD in Fig. 3(a). The simulated data points (black dots in Fig. 3(b)) yield $T_2^* = 21 \mu\text{s}$, which is very close to the experimentally determined value $T_2^* = 18 \mu\text{s}$ found in Fig. 2(b). In summary, comparing data covering more than 8 frequency decades, the excellent agreement demonstrates that charge noise dominates the qubit detuning noise in our device and transits from a $S(f) \propto 1/f^2$ dependence to a $S(f) \propto 1/f$ dependence around 10^{-3} Hz.

To complete our analysis of the detuning noise and the time-ensemble spin dephasing time T_2^* , we estimate the magnetic noise impact due to the residual non-zero spin nuclei in our device. We can compute the resulting T_2^* with (see Supplementary Note 2)

$$T_2^* = \frac{\hbar\sqrt{3N_S}}{p\gamma A\sqrt{2I(I+1)}}, \quad (7)$$

where N_S is the number of nuclei, p is the fraction of nuclei with finite nuclear spin, γ is the volume fraction of the wavefunction for which we want to calculate the influence on T_2^* , i.e. localized in the barrier or the quantum well. A is the hyperfine coupling constant per nucleus and I is the non-zero nuclear spin. In Ref.²², we measured the orbital splitting of this QD to be 2.5 meV. Assuming a harmonic potential, we calculate the size of the QD, taken to be the full-width-at-half-maximum of the ground state wavefunction. This yields a radius of ≈ 13 nm. By approximating the QD as a cylinder with height 6 nm we estimate the number of atoms in the QD volume to be $N_A = 1.6 \cdot 10^5$. From Schrödinger-Poisson simulations, we estimate the overlap with the SiGe barriers to be $\gamma_B \approx 0.1\%$. We calculate the number of non-zero nuclear spins, which are relevant for the hyperfine coupling with the qubit (i.e. are within the cylindrical volume assigned to the QD), for the residual 60 ppm ^{29}Si in the ^{28}Si strained QW layer, residual ^{29}Si and ^{73}Ge in the SiGe barriers with natural abundance of isotopes as, respectively:

$$N_{S,^{29}\text{Si}}^{\text{QW}} = p_{^{29}\text{Si}}^{\text{QW}}(1 - \gamma_B)N_A = 60 \cdot 10^{-6}(1 - \gamma_B)N_A \approx 9.6, \quad (8)$$

$$N_{S,^{29}\text{Si}}^{\text{barrier}} = p_{^{29}\text{Si}}^{\text{barrier}}\gamma_B N_A = 0.0467 \cdot 0.7 \cdot \gamma_B N_A \approx 5.2, \quad (9)$$

$$N_{S,^{73}\text{Ge}}^{\text{barrier}} = p_{^{73}\text{Ge}}^{\text{barrier}}\gamma_B N_A = 0.0776 \cdot 0.3 \cdot \gamma_B N_A \approx 3.7. \quad (10)$$

The coupling constants are $A_{\text{Si}} = 2.15 \mu\text{eV}$ and $A_{\text{Ge}} \approx 10 \cdot A_{\text{Si}}$ ^{18,19}, respectively, with $I_{^{29}\text{Si}} = 1/2$, $I_{^{73}\text{Ge}} = 9/2$. Assuming the spin baths to be in the ergodic limit, each subset of nuclear spin results in the following dephasing times: $T_2^*(^{\text{QW}}_{^{29}\text{Si}}) = 22 \mu\text{s}$, $T_2^*(^{\text{barrier}}_{^{29}\text{Si}}) = 30 \mu\text{s}$ and $T_2^*(^{\text{barrier}}_{^{73}\text{Ge}}) = 0.61 \mu\text{s}$. Notably, due to the strong hyperfine coupling of the ^{73}Ge in the barrier layers, the ^{73}Ge alone would dephase the qubit faster than observed in the experiment shown in Fig. 2(c). This apparent contradiction is resolved, if the correlation time of the ^{73}Ge nuclear spin bath is larger than a few hours and thus the ergodic limit is not reached in our $T_2^*(t_m)$ measurement.

In conclusion, we have shown that in a highly purified $^{28}\text{Si}/\text{SiGe}$ qubit device with 60 ppm residual ^{29}Si , the ^{73}Ge nuclear spins in the potential barrier do not dominantly contribute to the qubit dephasing time, despite their strong hyperfine coupling. We find the dynamics of the nuclear spin bath to be slower than 6 hours, similarly to observations for electrons bound to single phosphorus donors in 800 ppm residual ^{29}Si in the presence of the electron's Knight shift³⁰. Thus, the improvement potential of qubit dephasing times that can be expected from isotopical purification of the natural SiGe barrier is negligibly weak. In our device featuring a nanomagnet integrated into the gate layout for EDSR manipulation, charge noise is the dominant qubit noise source in a frequency range of more than 8 decades. In the low frequency regime, the charge and the qubit detuning noise present a $1/f^2$ dependence below $1 \cdot 10^{-3}$ Hz. Above, towards higher frequencies, both PSD transit to a $1/f$ dependence. This $1/f$ trend was recently also observed in a device featuring a micromagnet and 800 ppm ^{29}Si ¹². From the Hahn-echo experiment for our qubit detuning, we additionally deduce a remarkably high $T_2^{\text{echo}} = 128 \mu\text{s}$. We finally show T_2^* to clearly and monotonously decrease for measurement times increasing from seconds to several hours, in accordance with the absence of a roll-off in the charge noise PSD down to at least $5 \cdot 10^{-5}$ Hz. Our experimental $T_2^* \approx 18 \mu\text{s}$ for $t_m = 600$ s quantitatively results from the charge noise $S_C^{1/2}(1 \text{ Hz}) = 0.47 \mu\text{eV}/\sqrt{\text{Hz}}$, which falls within the range of 0.3 to $2 \mu\text{eV}/\sqrt{\text{Hz}}$ seen in literature^{31–34}. While the on-chip integration of a micro- or nanomagnet does not induce additional magnetic noise^{12,35}, minimizing the newly opened electric dephasing channel seems to be key for further significant improvement of spin qubit gate fidelities in highly purified ^{28}Si compared to devices avoiding integrated static magnetic field gradients^{13,14,36,37}.

See supplementary material for details of the measurement cycle, simulations of the nanomagnet and derivations for the T_2^* time in the ergodic limit and its dependence on measurement time.

This work has been funded by the German Research Foundation (DFG) within the projects BO 3140/4-1, 289786932

and the cluster of excellence "Matter and light for quantum computing" (ML4Q) as well as by the Federal Ministry of Education and Research under Contract No. FKZ: 13N14778. Project Si-QuBus received funding from the QuantERA ERA-NET Cofund in Quantum Technologies implemented within the European Union's Horizon 2020 Programme.

- ¹F. A. Zwanenburg, A. S. Dzurak, A. Morello, M. Y. Simmons, L. C. L. Hollenberg, G. Klimeck, S. Rogge, S. N. Coppersmith, and M. A. Eriksson, *Rev. Mod. Phys.* **85**, 961 (2013).
- ²L. V. C. Assali, H. M. Petrilli, R. B. Capaz, B. Koiller, X. Hu, and S. Das Sarma, *Phys. Rev. B* **83**, 165301 (2011).
- ³N. V. Abrosimov, D. G. Aref'ev, P. Becker, H. Bettin, A. D. Bulanov, M. F. Churbanov, S. V. Filimonov, V. A. Gavva, O. N. Godisov, A. V. Gusev, T. V. Kotereva, D. Nietzold, M. Peters, A. M. Potapov, H.-J. Pohl, A. Pramann, H. Riemann, P.-T. Scheel, R. Stosch, S. Wundrack, and S. Zakel, *Metrologia* **54**, 599 (2017).
- ⁴K. M. Itoh and H. Watanabe, *MRS Commun.* **4**, 143 (2014).
- ⁵A. Wild, J. Kierig, J. Sailer, J. W. Ager, E. E. Haller, G. Abstreiter, S. Ludwig, and D. Bougeard, *Appl. Phys. Lett.* **100**, 143110 (2012).
- ⁶J. T. Muhonen, J. P. Dehollain, A. Laucht, F. E. Hudson, R. Kalra, T. Sekiguchi, K. M. Itoh, D. N. Jamieson, J. C. McCallum, A. S. Dzurak, and A. Morello, *Nat. Nanotechnol.* **9**, 986 (2014).
- ⁷M. Veldhorst, J. C. C. Hwang, C. H. Yang, A. W. Leenstra, B. de Ronde, J. P. Dehollain, J. T. Muhonen, F. E. Hudson, K. M. Itoh, A. Morello, and A. S. Dzurak, *Nat. Nanotechnol.* **9**, 981 (2014).
- ⁸W. I. L. Lawrie, H. G. J. Eenink, N. W. Hendrickx, J. M. Boter, L. Petit, S. V. Amitonov, M. Lodari, B. Paquelet Wuetz, C. Volk, S. Philips, G. Droulers, N. Kalhor, F. van Riggelen, D. Brousse, A. Sammak, L. M. K. Vandersypen, G. Scappucci, and M. Veldhorst, *arXiv*, 1909.06575 (unpublished).
- ⁹M. Veldhorst, C. H. Yang, J. C. C. Hwang, W. Huang, J. P. Dehollain, J. T. Muhonen, S. Simmons, A. Laucht, F. E. Hudson, K. M. Itoh, A. Morello, and A. S. Dzurak, *Nature* **526**, 410 (2015).
- ¹⁰D. M. Zajac, A. J. Sigillito, M. Russ, F. Borjans, J. M. Taylor, G. Burkard, and J. R. Petta, *Science* **359**, 439 (2018).
- ¹¹T. F. Watson, S. G. J. Philips, E. Kawakami, D. R. Ward, P. Scarlino, M. Veldhorst, D. E. Savage, M. G. Lagally, M. Friesen, S. N. Coppersmith, M. A. Eriksson, and L. M. K. Vandersypen, *Nature* **555**, 633 (2018).
- ¹²J. Yoneda, K. Takeda, T. Otsuka, T. Nakajima, M. R. Delbecq, G. Allison, T. Honda, T. Kadera, S. Oda, Y. Hoshi, N. Usami, K. M. Itoh, and S. Tarucha, *Nat. Nanotechnol.* **13**, 102 (2018).
- ¹³C. H. Yang, K. W. Chan, R. Harper, W. Huang, T. Evans, J. C. C. Hwang, B. Bensen, A. Laucht, T. Tanttu, H. F. E., S. T. Flammia, K. M. Itoh, A. Morello, S. D. Bertlett, and A. S. Dzurak, *Nat. Electronics* **2**, 151 (2019).
- ¹⁴W. Huang, C. H. Yang, K. W. Chan, T. Tanttu, B. Hensen, R. C. C. Leon, M. A. Fogarty, J. C. C. Hwang, F. E. Hudson, K. M. Itoh, A. Morello, A. Laucht, and A. S. Dzurak, *Nature* **569**, 532 (2019).
- ¹⁵F. H. L. Koppens, C. Buizert, K. J. Tielrooij, I. T. Vink, K. C. Nowack, T. Meunier, L. P. Kouwenhoven, and L. M. K. Vandersypen, *Nature* **442**, 766 (2006).
- ¹⁶M. Pioro-Ladrière, T. Obata, Y. Tokura, Y.-S. Shin, T. Kubo, K. Yoshida, T. Taniyama, and S. Tarucha, *Nat. Phys.* **4**, 776 (2008).
- ¹⁷R. Zhao, T. Tanttu, K. Y. Tan, B. Hensen, K. W. Chan, J. C. C. Hwang, R. C. C. Leon, C. H. Yang, W. Gilbert, F. E. Hudson, K. M. Itoh, A. A. Kiselev, T. D. Ladd, A. Morello, A. Laucht, and A. S. Dzurak, *arXiv*, 1812.08347 (unpublished).
- ¹⁸D. K. Wilson, *Phys. Rev.* **134**, A265 (1964).
- ¹⁹W. M. Witzel, R. Rahman, and M. S. Carroll, *Phys. Rev. B* **85**, 205312 (2012).
- ²⁰O. E. Dial, M. D. Shulman, S. P. Harvey, H. Bluhm, V. Umansky, and A. Yacoby, *Phys. Rev. Lett.* **110**, 146804 (2013).
- ²¹G. Petersen, E. A. Hoffmann, D. Schuh, W. Wegscheider, G. Giedke, and S. Ludwig, *Phys. Rev. Lett.* **110**, 177602 (2013).
- ²²A. Hollmann, T. Struck, V. Langrock, A. Schmidbauer, F. Schauer, K. Sawano, H. Riemann, N. V. Abrosimov, D. Bougeard, and L. R. Schreiber, *arXiv*, 1907.04146 (unpublished).
- ²³J. Lu, F. Hoehne, A. R. Stegner, L. Dreher, M. Stutzmann, M. S. Brandt, and H. Huebl, *Phys. Rev. B* **83**, 235201 (2011).
- ²⁴R. Hanson, L. P. Kouwenhoven, J. R. Petta, S. Tarucha, and L. M. K. Vandersypen, *Rev. Mod. Phys.* **79**, 1217 (2007).
- ²⁵L. Cywiński, W. M. Witzel, and S. Das Sarma, *Phys. Rev. Lett.* **102**, 057601 (2009).
- ²⁶L. Cywiński, *Acta Phys. Pol. A* **119**, 576 (2011).
- ²⁷D. J. Reilly, J. M. Taylor, E. A. Laird, J. R. Petta, C. M. Marcus, M. P. Hanson, and A. C. Gossard, *Phys. Rev. Lett.* **101**, 236803 (2008).
- ²⁸F. K. Malinowski, F. Martins, L. Cywiński, M. S. Rudner, P. D. Nissen, S. Fallahi, G. C. Gardner, M. J. Manfra, C. M. Marcus, and F. Kuemmeth, *Phys. Rev. Lett.* **118**, 177702 (2017).
- ²⁹K. Takeda, T. Obata, Y. Fukuoka, W. M. Akhtar, J. Kamioka, T. Kadera, S. Oda, and S. Tarucha, *Appl. Phys. Lett.* **102**, 123113 (2013).
- ³⁰M. T. Mądzik, T. D. Ladd, F. E. Hudson, K. M. Itoh, A. M. Jakob, B. C. Johnson, D. N. Jamieson, J. C. McCallum, A. S. Dzurak, A. Laucht, and A. Morello, *arXiv*, 1907.11032 (unpublished).
- ³¹B. M. Freeman, J. S. Schoenfeld, and H. Jiang, *Applied Physics Letters* **108**, 253108 (2016).
- ³²E. J. Connors, J. Nelson, H. Qiao, L. F. Edge, and J. M. Nichol, *arXiv*, 1907.07549 (unpublished).
- ³³L. Petit, J. M. Boter, H. G. J. Eenink, G. Droulers, M. L. V. Tagliaferri, R. Li, D. P. Franke, K. J. Singh, J. S. Clarke, R. N. Schouten, V. V. Dobrovitski, L. M. K. Vandersypen, and M. Veldhorst, *Phys. Rev. Lett.* **121**, 076801 (2018).
- ³⁴X. Mi, S. Kohler, and J. R. Petta, *Phys. Rev. B* **98**, 161404 (2018).
- ³⁵R. Neumann and L. R. Schreiber, *J. Appl. Phys.* **117**, 193903 (2015).
- ³⁶B. Thorgrimsson, D. Kim, Y.-C. Yang, L. W. Smith, C. B. Simmons, D. R. Ward, R. H. Foote, J. Corrigan, D. E. Savage, M. G. Lagally, M. Friesen, S. N. Coppersmith, and M. A. Eriksson, *npj Quantum Information* **3**, 32 (2017).
- ³⁷R. W. Andrews, C. Jones, D. M. Reed, A. M. Jones, S. D. Ha, M. P. Jura, J. Kerckhoff, M. Levendoff, S. Meenehand, S. T. Merkel, A. Smith, B. Sun, A. J. Weinstein, M. T. Rakher, T. D. Ladd, and M. G. Borselli, *Nat. Nanotechnol.* **14**, 747 (2019).